LETTER

doi:10.1038/nature13155

A ring system detected around the Centaur (10199) Chariklo

F. Braga-Ribas[1], B. Sicardy[2], J. L. Ortiz[3], C. Snodgrass[4], F. Roques[2], R. Vieira-Martins[1,5,6], J. I. B. Camargo[1], M. Assafin[5], R. Duffard[3], E. Jehin[7], J. Pollock[8], R. Leiva[9], M. Emilio[10], D. I. Machado[11,12], C. Colazo[13,14], E. Lellouch[2], J. Skottfelt[15,16], M. Gillon[7], N. Ligier[2], L. Maquet[2], G. Benedetti-Rossi[1], A. Ramos Gomes Jr[5], P. Kervella[2], H. Monteiro[17], R. Sfair[18], M. El Moutamid[2,6], G. Tancredi[19,20], J. Spagnotto[21], A. Maury[22], N. Morales[3], R. Gil-Hutton[23], S. Roland[19], A. Ceretta[20,24], S.-h. Gu[25,26], X.-b. Wang[25,26], K. Harpsøe[15,16], M. Rabus[9,27], J. Manfroid[7], C. Opitom[7], L. Vanzi[28], L. Mehret[10], L. Lorenzini[11], E. M. Schneiter[14,29,30,31], R. Melia[14], J. Lecacheux[2], F. Colas[6], F. Vachier[6], T. Widemann[2], L. Almenares[19,20], R. G. Sandness[22], F. Char[32], V. Perez[19,20], P. Lemos[20], N. Martinez[19,20], U. G. Jørgensen[15,16], M. Dominik[33], F. Roig[1], D. E. Reichart[34], A. P. LaCluyze[34], J. B. Haislip[34], K. M. Ivarsen[34], J. P. Moore[34], N. R. Frank[34] & D. G. Lambas[14,30]

Hitherto, rings have been found exclusively around the four giant planets in the Solar System[1]. Rings are natural laboratories in which to study dynamical processes analogous to those that take place during the formation of planetary systems and galaxies. Their presence also tells us about the origin and evolution of the body they encircle. Here we report observations of a multichord stellar occultation that revealed the presence of a ring system around (10199) Chariklo, which is a Centaur—that is, one of a class of small objects orbiting primarily between Jupiter and Neptune—with an equivalent radius of 124 ± 9 kilometres (ref. 2). There are two dense rings, with respective widths of about 7 and 3 kilometres, optical depths of 0.4 and 0.06, and orbital radii of 391 and 405 kilometres. The present orientation of the ring is consistent with an edge-on geometry in 2008, which provides a simple explanation for the dimming[3] of the Chariklo system between 1997 and 2008, and for the gradual disappearance of ice and other absorption features in its spectrum over the same period[4,5]. This implies that the rings are partly composed of water ice. They may be the remnants of a debris disk, possibly confined by embedded, kilometre-sized satellites.

Chariklo is the largest known Centaur orbiting in a region between Saturn and Uranus, and has an orbital eccentricity of 0.175 and a semi-major axis of 15.8 astronomical units (1 AU is the Earth–Sun distance). It may be a former trans-Neptunian object that has been recently (less than 10 Myr ago) scattered by gravitational perturbations from Uranus[6]. No clear detection of Chariklo's rotation has been made so far. Its surface is very dark, with a geometric albedo[2] of 0.035 ± 0.011, and it is subject to long-term spectral and photometric variabilities[3–5], although no cometary activity has ever been reported.

An occultation of an $R = 12.4$ mag star by Chariklo was predicted[7] to cross South America on 3 June 2013 (Extended Data Figs 1 and 2). We obtained data from sites in Brazil, Argentina, Uruguay and Chile (Extended Data Table 1). Although the occultation by Chariklo itself was recorded at three sites in Chile, seven sites detected a total of thirteen rapid stellar flux interruptions (secondary events), two of them being resolved into two sub-events by the Danish 1.54-m telescope at the European Southern Observatory at La Silla, Chile (Fig. 1).

Displayed in the Extended Data and analysed in the Supplementary Information, all those secondary events (Extended Data Tables 2 and 3) can be readily explained by the presence of two narrow and azimuthally homogeneous rings (Fig. 2), whose widths and optical depths are given in Table 1. Even if the events were generally not resolved (Extended Data Fig. 3), their depths provide a measure of the integrated light loss of the events, which in turn depends on the local geometry of the occultation in the plane of the sky. The fact that all the events are consistent with an azimuthally homogeneous ring system makes other interpretations, such as an ensemble of cometary jets, very unlikely.

Other evidence supports our interpretation of a flat circular ring system around Chariklo. The ellipse fitted to the secondary events provides two possible ring pole positions (Table 1 and Extended Data Table 4). Our preferred solution is the one in which the rings had an opening angle of 60° in 1996–1997 and vanished from view as they were observed edge-on in 2008, owing to the orbital motion of Chariklo relative to the Earth. This provides a simple explanation for the gradual dimming of Chariklo's system, by a factor of 1.75, during that period[3]. Further evidence is that the 2-μm water-ice band and the spectral slope below 0.55 μm gradually disappeared[4,5] between 1997 and 2008, implying that water ice is present in the rings. Observations made in 2013 show that the system has brightened by a factor of about 1.5 since 2008, and that the water-ice band is detectable again, supporting our interpretation (R.D. *et al.*, manuscript in preparation).

[1]Observatório Nacional/MCTI, Rua General José Cristino 77, CEP 20921-400 Rio de Janeiro, RJ, Brazil. [2]LESIA, Observatoire de Paris, CNRS UMR 8109, Université Pierre et Marie Curie, Université Paris-Diderot, 5 place Jules Janssen, F-92195 Meudon Cedex, France. [3]Instituto de Astrofísica de Andalucía, CSIC, Apartado 3004, 18080 Granada, Spain. [4]Max Planck Institute for Solar System Research, Justus-von-Liebig-Weg 3, 37077 Göttingen, Germany. [5]Observatório do Valongo/UFRJ, Ladeira Pedro Antonio 43, CEP 20.080-090 Rio de Janeiro, RJ, Brazil. [6]Observatoire de Paris, IMCCE, UPMC, CNRS, 77 Avenue Denfert-Rochereau, 75014 Paris, France. [7]Institut d'Astrophysique de l'Université de Liège, Allée du 6 Août 17, B-4000 Liège, Belgium. [8]Physics and Astronomy Department, Appalachian State University, Boone, North Carolina 28608, USA. [9]Instituto de Astrofísica, Facultad de Física, Pontificia Universidad Católica de Chile, Avenida Vicuña Mackenna 4860, Santiago 7820436, Chile. [10]Universidade Estadual de Ponta Grossa, O.A. - DEGEO, Avenida Carlos Cavalcanti 4748, Ponta Grossa 84030-900, PR, Brazil. [11]Polo Astronômico Casimiro Montenegro Filho/FPTI-BR, Avenida Tancredo Neves 6731, CEP 85867-900, Foz do Iguaçu, PR, Brazil. [12]Universidade Estadual do Oeste do Paraná (Unioeste), Avenda Tarquínio Joslin dos Santos, 1300, CEP 85870-650, Foz do Iguaçu, PR, Brazil. [13]Ministerio de Educación de la Provincia de Córdoba, Santa Rosa 751, Córdoba 5000, Argentina. [14]Observatorio Astronómico, Universidad Nacional de Córdoba, Laprida 854, Córdoba 5000, Argentina. [15]Niels Bohr Institute, University of Copenhagen, Juliane Maries vej 30, 2100 Copenhagen, Denmark. [16]Centre for Star and Planet Formation, Geological Museum, Øster Voldgade 5, 1350 Copenhagen, Denmark. [17]Instituto de Física e Química, Avenida BPS 1303, CEP 37500-903, Itajubá, MG, Brazil. [18]UNESP - Universidade Estadual Paulista, Avenida Ariberto Pereira da Cunha, 333, CEP 12516-410 Guaratinguetá, SP, Brazil. [19]Observatorio Astronomico Los Molinos, DICYT, MEC, 12400 Montevideo, Uruguay. [20]Departamento de Astronomia, Facultad Ciencias, Universidad de la República, 11300 Montevideo, Uruguay. [21]Observatorio El Catalejo, Mussio 255, Santa Rosa, La Pampa 6300, Argentina. [22]San Pedro de Atacama Celestial Explorations, Casilla 21, San Pedro de Atacama 1410000, Chile. [23]Complejo Astronómico El Leoncito (CASLEO) and San Juan National University, Avenida España 1512 sur, J5402DSP, San Juan, Argentina. [24]Observatorio del IPA, Consejo de Formación en Educación, 11800 Montevideo, Uruguay. [25]Yunnan Observatories, Chinese Academy of Sciences, Kunming 650011, China. [26]Key Laboratory for the Structure and Evolution of Celestial Objects, Chinese Academy of Sciences, Kunming 650011, China. [27]Max Planck Institute for Astronomy, Königstuhl 17, 69117 Heidelberg, Germany. [28]Department of Electrical Engineering and Center of Astro-Engineering, Pontificia Universidad Católica de Chile, Avenida Vicuña Mackenna 4860, Santiago 7820436, Chile. [29]Consejo Nacional de Investigaciones Científicas y Técnicas (CONICET), Córdoba 5000, Argentina. [30]Instituto de Astronomía Teórica y Experimental IATE–CONICET, Córdoba 5000, Argentina. [31]Facultad de Ciências Exactas, Físicas y Naturales, Universidad Nacional de Córdoba (UNC), Córdoba 5000, Argentina. [32]Unidad de Astronomía, Facultad de Ciencias Básicas, Universidad de Antofagasta, Avenida Angamos 601, Antofagasta, Region II, Chile. [33]Scottish Universities Physics Alliance, University of St Andrews, School of Physics and Astronomy, North Haugh, St Andrews KY16 9SS, UK. [34]Department of Physics and Astronomy, University of North Carolina - Chapel Hill, North Carolina 27599, USA.

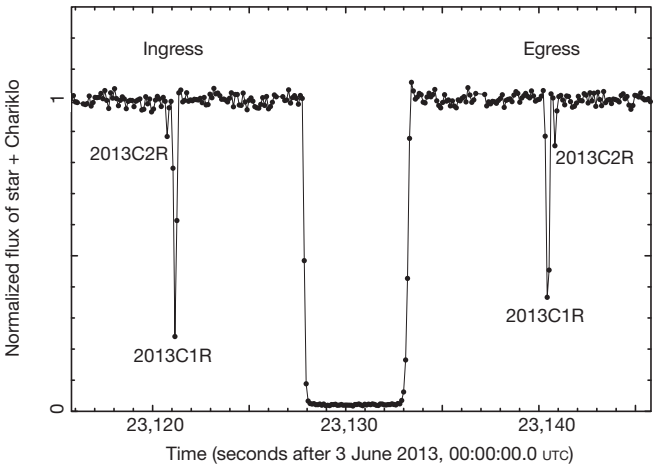

Figure 1 | Light curve of the occultation by the Chariklo system. The data were taken with the Danish 1.54-m telescope (La Silla) on 3 June 2013, at a rate of almost 10 Hz and with a long-pass filter and a cut-off below 650 nm, limited at long wavelengths by the sensitivity of the charge-coupled-device chip (Supplementary Information). Aperture photometry provided the flux from the target star and a fainter nearby reference star. Low-frequency sky transparency variations were removed by dividing the target flux by an optimal running average of 87 data points (8.7 s) of the reference star, resulting in a final signal-to-noise ratio of 64 per data point. The sum of the stellar and Chariklo fluxes has been normalized to unity outside the occultation. The central drop is caused by Chariklo, and two secondary events, 2013C1R and 2013C2R, are observed, one at ingress (before the main Chariklo occultation) and then at egress (after the main occultation). A more detailed view of these ring events is shown in Fig. 3.

Owing to its higher acquisition rate (10 Hz), the Lucky Imager camera[8,9] of the Danish 1.54-m telescope actually resolved the secondary events into two rings, denoted 2013C1R and 2013C2R (C1R and C2R for short) in Figs 1 and 3. We use the terms ingress and egress refer to the first and, respectively, second of a pair of ring events at a given site. All the Danish events are satisfactorily fitted by sharp-edged ring models whose radial widths (W) in the ring plane and normal optical depths (τ_N) are listed in Table 1. We also provide the equivalent depths ($E_\tau = W\tau_N$), which can be related to the amount of material contained in the ring[10]. C2R is about 40% narrower than C1R, and contains about 12 times less material. We note that no material is detected in the gap between C1R and C2R, up to a limit of 0.004 in normal optical depth and 0.05 km in equivalent depth (Table 1 and Extended Data Table 4).

By analogy with Saturn's A ring[11] or the dense rings of Uranus[12], we estimate that the surface density of C1R lies in the range 30–100 g cm^{-2} (Supplementary Information). Then, the mass of C1R is equivalent to that of an icy body with a radius of roughly 1 km, whereas C2R corresponds to a body of half that size. If the photometric variability of Chariklo's system between 1997 and 2008 is entirely due to the ring changing geometry[3], we estimate the ring reflectivity to be $I/F \approx 0.09 \pm 0.04$ (I is the intensity of light reflected by the surface and πF is the incident solar flux density). Thus, Chariklo's ring particles would be significantly brighter than those of Uranus's rings[13] ($I/F \approx 0.05$), but would be significantly darker than those of Saturn's A ring[14] ($I/F \approx 0.3$). We note that, if part of the photometric variability is caused by Chariklo itself, then the ring material would be darker than estimated above (Supplementary Information).

Constraints on Chariklo's limb shape are based on only two occultation chords (Supplementary Information and Extended Data Table 5). Our simplest model describes an oblate Chariklo surrounded by a circular equatorial ring system (Extended Data Table 6). The fitted limb (Fig. 2) has an equivalent radius of 127 km (the radius of an equivalent

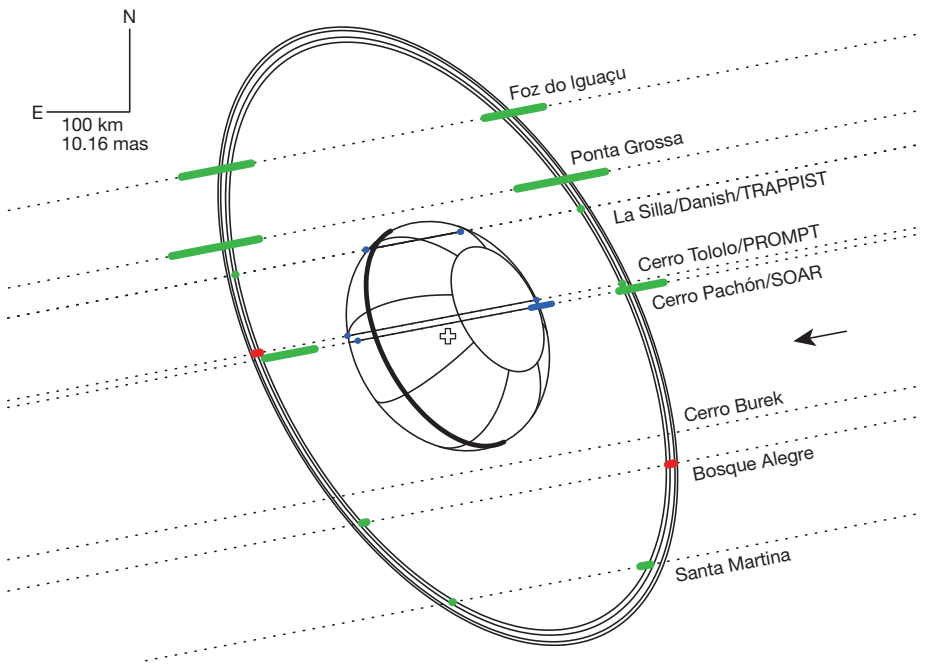

Figure 2 | Chariklo ring system. The dotted lines are the trajectories of the star relative to Chariklo in the plane of the sky, as observed from eight sites (Supplementary Information), the arrow indicating the direction of motion. The green segments represent the locations of ring C1R observed at each station (1σ uncertainty). For clarity, we have not plotted the detections made at the TRAPPIST and 0.275-m telescopes (at La Silla and Bosque Alegre, respectively) because they have larger error bars than their local counterparts, and would supersede the corresponding green segments. Two ring events occurred during camera readout times (red segments) at Bosque Alegre and Cerro Tololo, and also provide constraints on the ring orbit. The ring events are only marginally detected at Cerro Burek, but the signal-to-noise ratio is not sufficient to put further constraints on the ring orbit and equivalent width. An elliptical fit to the green and red segments (excluding, because of timing problems (Supplementary Information), the SOAR events at Cerro Pachón) provides the centre of the rings (open cross), as well as their sizes, opening angle and orientation (Table 1). Chariklo's limb has been fitted to the two chords' extremities (blue segments) obtained at La Silla and Cerro Tololo, assuming that the centres of Chariklo and the rings, as well as their position angles, coincide. This is expected if Chariklo is a spheroid, with a circular ring orbiting in the equatorial plane (see text and Supplementary Information).

Table 1 | Ring physical parameters

	Radial width, W (km)	Normal optical depth, τ_N	Equivalent depth, $E_\tau = W\tau_N$ (km)
Ring C1R, Danish ingress	6.16 ± 0.11	0.449 ± 0.009	2.77 ± 0.04
Ring C1R, Danish egress	7.17 ± 0.14	0.317 ± 0.008	2.28 ± 0.03
Ring C2R, Danish ingress	$3.6^{+1.3}_{-2.0}$	$0.05^{+0.06}_{-0.01}$	0.18 ± 0.03
Ring C2R, Danish egress	$3.4^{+1.1}_{-1.4}$	$0.07^{+0.05}_{-0.03}$	0.24 ± 0.02
Ring C1R radius (km)		390.6 ± 3.3	
Ring C2R radius (km)		404.8 ± 3.3	
Radial separation of rings C1R and C2R (km)		14.2 ± 0.2	
Gap between rings C1R and C2R (km)		8.7 ± 0.4 ($E_\tau < 0.05$ km, $\tau_N < 0.004$)	
Opening angle, B (°)		$+33.77 \pm 0.41$	
Position angle, P (°)		-61.54 ± 0.14 (preferred) or 118.46 ± 0.14	
	Pole position (equatorial J2000)		
	Solution 1 (preferred)		Solution 2
Right ascension, α_p	10 h 05.2 min ± 2.0 min		01 h 47.8 min ± 1.2 min
Declination, δ_p	41° 29′ ± 13′		03° 26′ ± 19′

The geocentric distance of Chariklo's system at the moment of the occultation, $D = 2.031 \times 10^9$ km, provides a scale of 9,846 km arcsec^{-1} in the plane of the sky. All the secondary events apart from those of the Danish 1.54-m telescope (Fig. 3) are satisfactorily fitted by a model where the rings C1R and C2R have widths and optical depths that are averages of the Danish ingress and egress values given above, that is, $W_{C1R} = 6.6$ km, $\tau_{N,C1R} = 0.38$, $W_{C2R} = 3.4$ km and $\tau_{N,C2R} = 0.06$ (Supplementary Information). The ring opening angle, B, is the absolute value of the elevation of the observer above the ring plane. The position angle, P, is the angle between celestial north and the semi-minor axis of the ring projected in the plane of the sky, counted positively from celestial north to celestial east. By convention, it refers to the projected semi-major axis that corresponds to superior conjunction. The solution that best explains the photometric and spectral variations of Chariklo's system[3–5] is chosen as preferred (see text).

spherical body; see Supplementary Information), consistent with the value derived from thermal data[2], 124 ± 9 km, thus supporting our model.

From the Roche critical density limit[15], we estimate that typical densities for Chariklo and ring particles are consistent with the present ring locations (Supplementary Information). Moreover, an unperturbed ring several kilometres in width and of thickness h should spread, owing to interparticle collisions[16], in $10^4/h^2$ years (Supplementary Information), or a few thousand years, assuming h of a few metres (by analogy with Saturn's rings). Furthermore, Poynting–Robertson drag[16] should spread sub-centimetre particles in a few million years at most (Supplementary Information). Thus, the rings are either very young or actively confined. A confinement mechanism may be provided by kilometre-sized 'shepherd satellites' that would have a mass comparable to that of the rings (Supplementary Information).

We do not know if rings around minor bodies stem from a generic, yet unknown, process, or are exceptional features. We note that many stellar occultations by main-belt asteroids and more than ten trans-Neptunian events[17–20] have not revealed rings so far (nor have direct images). Stellar occultations and appulses involving (2060) Chiron (a Centaur similar in size to Chariklo) in 1993 and 1994 revealed a narrow, jet-like feature and diffuse material around that object[21,22]. This was interpreted as material ejected from the surface, partly on the basis that Chiron is known to be an active, comet-like object. It is unclear whether the detection of material around both objects is a mere coincidence, or whether they share a common physical process (noting that no cometary activity has been detected around Chariklo).

About 5% of the Centaur and trans-Neptunian population[23] are known to have satellites. Although the large satellites are thought to result from three-body captures, their small counterparts are more likely to form from impacts[24], or rotational disruptions[25], and possibly re-accretion from a disk remaining after that event. So far, no observations have shown satellites around Chariklo (the rings span at most 0.04″ around the primary object, making direct detections of associated small satellites a challenge). Several origins for Chariklo's rings can be proposed, all relying on a debris disk in which the largest fragments acted as shepherds for the smaller material. The first possibility is that an impactor excavated icy material from Chariklo's outer layers, destroyed a pre-existing satellite or was itself disrupted during the impact. The second is that a debris disk formed from a rotational disruption of the main body or was fed by cometary-like activity. Third, two pre-existing satellites

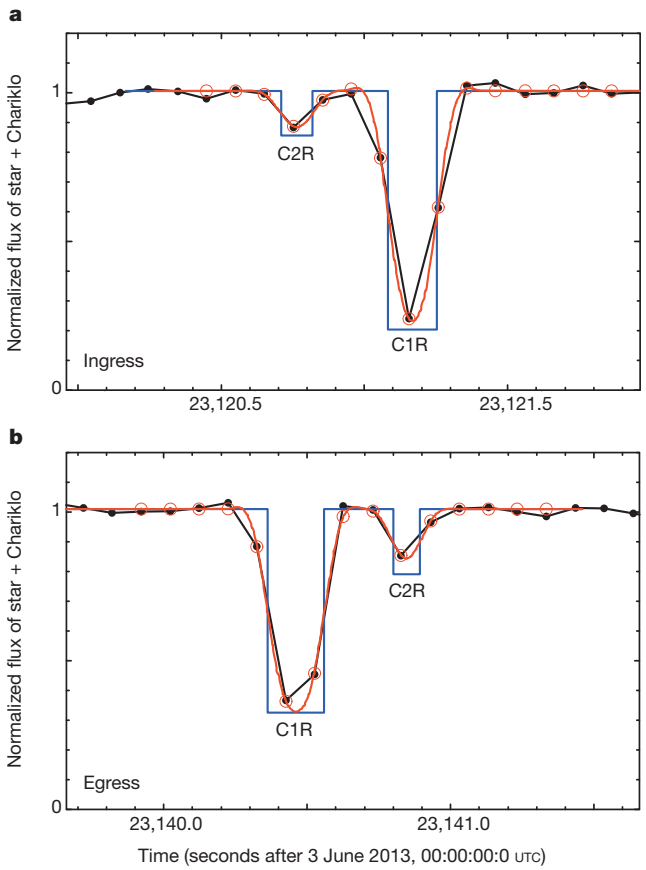

Figure 3 | Fits to the Danish ring events. **a**, **b**, The red curves are synthetic occultation profiles produced by semi-transparent bands with square-well profiles (the blue lines), after convolution by Fresnel diffraction, observed bandwidth, the stellar radius projected at Chariklo, and the finite integration time. The open red circles are the values of the model for the times corresponding to the observed data points (black points) at the ingress (**a**) and egress (**b**). The χ^2 values per degree of freedom of the fits to the four ring events vary from 0.4 to 1.2 (Extended Data Table 2). This indicates satisfactory fits, and shows that the events are compatible with sharp-edged rings. The resulting widths and optical depths of rings C1R and C2R are listed in Table 1, after the appropriate projections into the plane of the rings have been performed. Extended Data Table 3 shows that the widths and optical depths of C1R at the Danish 1.54-m telescope differ moderately but significantly between ingress and egress. The equivalent depth of C1R changes by 21% between ingress and egress. Similar variations are observed in Uranus's narrow rings, and might be associated with normal mode oscillations that azimuthally modulate the width and optical depth of the rings[10]. Differences between C2R ingress and egress are marginally significant.

might have collided through a mechanism yet to be explained. Finally, a retrograde satellite might have migrated inwards and eventually been disrupted by tidal forces.

We note that the mass and angular momentum of the rings and their hypothetical shepherds are very small (by a factor of less than 10^{-5}) compared with that of Chariklo. The typical escape velocity at the surface of Chariklo is $\sim$0.1 km s^{-1}. Thus, if an impact from an outsider generated the rings, it must have struck at low velocity. Whereas the impact velocities in the main belt of asteroids are of the order of 5 km s^{-1}, they are $\sim$1 km s^{-1} in the outer Solar System, and were even lower before the Kuiper Belt was dynamically excited[26], which may explain why no rings have yet been found around main-belt asteroids. Finally, Chariklo's orbit is perturbed by Uranus, which transferred the Centaur from the trans-Neptunian region less than $\sim$10 Myr ago[6]. As estimated in Supplementary Information, a very close encounter at about five Uranus radii is actually necessary to disrupt the ring system. Such an event has a small probability of occurrence[27], which supports the possibility that the rings formed in the trans-Neptunian region and survived the transfer episode.

Received 23 December 2013; accepted 11 February 2014.
Published online 26 March 2014.

1. Tiscareno, M. S. in *Planets, Stars and Stellar Systems* Vol. 3 *Solar and Stellar Planetary Systems* (eds Oswalt, T. D., French, L. M. & Kalas, P.) 309–375 (Springer, 2013).
2. Fornasier, S. *et al.* TNOs are cool: A survey of the trans-Neptunian region VIII. Combined Herschel PACS and SPIRE observations of nine bright targets at 70–500 μm. *Astron. Astrophys.* **555,** A15 (2013).
3. Belskaya, I. N. *et al.* Polarimetry of Centaurs (2060) Chiron, (5145) Pholus and (10199) Chariklo. *Icarus* **210,** 472–479 (2010).
4. Guilbert, A. *et al.* A portrait of Centaur 10199 Chariklo. *Astron. Astrophys.* **501,** 777–784 (2009).
5. Guilbert-Lepoutre, A. A thermal evolution model of Centaur 10199 Chariklo. *Astron. J.* **141,** 103 (2011).
6. Horner, J., Evans, N. W. & Bailey, M. E. Simulations of the population of Centaurs - I. The bulk statistics. *Mon. Not. R. Astron. Soc.* **354,** 798–810 (2004).
7. Camargo, J. I. B. *et al.* Candidate stellar occultations by Centaurs and trans-Neptunian objects up to 2014. *Astron. Astrophys.* **561,** A37 (2014).
8. Harpsøe, K. B. W., Jørgensen, U. G., Andersen, M. I. & Grundahl, F. High frame rate imaging based photometry. Photometric reduction of data from electron-multiplying charge coupled devices (EMCCDs). *Astron. Astrophys.* **542,** A23 (2012).
9. Skottfelt, J. *et al.* EMCCD photometry reveals two new variable stars in the crowded central region of the globular cluster NGC 6981. *Astron. Astrophys.* **553,** A111 (2013).
10. French, R. G., Nicholson, P. D., Porco, C. C. & Marouf, E. A. in *Uranus* (eds Bergstralh, J. T., Miner, E. D. & Matthews, M. S.) 327–409 (Univ. Arizona Press, 1991).
11. Colwell, J. E. *et al.* in *Saturn from Cassini-Huygens* (eds Dougherty, M. K., Esposito, L. W. & Krimigis, S. M.) 375–412 (Springer, 2009).
12. Esposito, L. W., Brahic, A., Burns, J. A. & Marouf, E. A. in *Uranus* (eds Bergstralh, J. T., Miner, E. D. & Matthews, M. S.) 410–465 (Univ. Arizona Press, 1991).
13. Karkoschka, E. Comprehensive photometry of the rings and 16 satellites of Uranus with the Hubble Space Telescope. *Icarus* **151,** 51–68 (2001).
14. Hedman, M. M. *et al.* Connections between spectra and structure in Saturn's main rings based on Cassini VIMS data. *Icarus* **223,** 105–130 (2013).
15. Tiscareno, M. S., Hedman, M. M., Burns, J. A. & Castillo-Rogez, J. Compositions and origins of outer planet systems: insights from the Roche critical density. *Astrophys. J.* **765,** L28 (2013).
16. Goldreich, P. & Tremaine, S. Towards a theory for the Uranian rings. *Nature* **277,** 97–99 (1979).
17. Elliot, J. L. *et al.* Size and albedo of Kuiper belt object 55636 from a stellar occultation. *Nature* **465,** 897–900 (2010).
18. Sicardy, B. *et al.* A Pluto-like radius and a high albedo for the dwarf planet Eris from an occultation. *Nature* **478,** 493–496 (2011).
19. Ortiz, J. L. *et al.* Albedo and atmospheric constraints of dwarf planet Makemake from a stellar occultation. *Nature* **491,** 566–569 (2012).
20. Braga-Ribas, F. *et al.* The size, shape, albedo, density, and atmospheric limit of Transneptunian object (50000) Quaoar from multi-chord stellar occultations. *Astrophys. J.* **773,** 26 (2013).
21. Bus, S. J. *et al.* Stellar occultation by 2060 Chiron. *Icarus* **123,** 478–490 (1996).
22. Elliot, J. L. *et al.* Jet-like features near the nucleus of Chiron. *Nature* **373,** 46–49 (1995).
23. Brunini, A. On the dynamical evolution and end states of binary Centaurs. *Mon. Not. R. Astron. Soc.* **437,** 2297–2302 (2014).
24. Noll, K. S., Grundy, W. M., Chiang, E. I., Margot, J.-L. & Kern, S. D. in *The Solar System Beyond Neptune* (eds Barucci, M. A., Boehnhardt, H., Cruikshank, D. P. & Morbidelli, A.) 345–363 (Univ. Arizona Press, 2008).
25. Ortiz, J. L. *et al.* Rotational fission of trans-Neptunian objects: the case of Haumea. *Mon. Not. R. Astron. Soc.* **419,** 2315–2324 (2012).
26. Ćuk, M., Ragozzine, D. & Nesvorný, D. On the dynamics and origin of Haumea's moons. *Astron. J.* **146,** 89 (2013).
27. Nogueira, E., Brasser, R. & Gomes, R. Reassessing the origin of Triton. *Icarus* **214,** 113–130 (2011).

Supplementary Information is available in the online version of the paper.

Acknowledgements We thank S. Fornasier, I. Belskaya, B. Carry, E. Nogueira, P. Michel and A. Morbidelli for the discussions that helped to interpret our results. We also thank J. A. Burns for comments that helped to improve the paper. F.B.-R. acknowledges LIneA (Laboratório Interinstitucional de e-Astronomia) for hosting the campaign webpage and the support (grant 150541/2013-9) of CNPq, Brazil. Operation of the Danish 1.54-m telescope is financed by a grant to U.G.J. by the Danish Natural Science Research Council (FNU) and by the Centre for Star and Planet Formation (StarPlan). F. Colas, J.L., L. Maquet, F. Roques, B.S., F.V. and T.W. acknowledge support from the French grant 'Beyond Neptune II'. J.L.O., R.D. and N. Morales acknowledge funding from Spanish AYA grants and FEDER funds. S.-h.G. and X.-b.W. are grateful for financial support from the National Natural Science Foundation of China through grants 10873031 and 11073051. M.D. is a Royal Society University Research Fellow at St Andrews University. TRAPPIST is a project funded by the Belgian Fund for Scientific Research (FRS-FNRS) with the participation of the Swiss National Science Foundation (SNF). E.J. and M.G. are FNRS Research Associates, J.M. is FNRS Research Director. C.O. thanks the Belgian FNRS for funding her PhD thesis. J.I.B.C., M.A. and R.V.-M. acknowledge CNPq grants 302657/2010-0, 482080/2009-4 478318/2007-3 and 304124/2007-9, respectively. The Universidad Católica Observatory (UCO) Santa Martina is operated by the Pontifícia Universidad Católica de Chile (PUC). C.S. received funding from the European Union Seventh Framework Programme (FP7/2007-2013) under grant agreement no. 268421. M.R. acknowledges support from FONDECYT postdoctoral fellowship 3120097. This work is partly based on observations made at the Pico dos Dias Observatory from the National Laboratory of Astrophysics (OPD/LNA) – Brazil; and partly based on observations obtained at the Southern Astrophysical Research (SOAR) telescope, which is a joint project of the Ministério da Ciência, Tecnologia, e Inovação (MCTI) da República Federativa do Brasil, the US National Optical Astronomy Observatory (NOAO), the University of North Carolina at Chapel Hill (UNC-CH) and Michigan State University (MSU). This publication makes use of data products from the Two Micron All Sky Survey, a joint project of the University of Massachusetts and the Infrared Processing and Analysis Center/California Institute of Technology, funded by the National Aeronautics and Space Administration (NASA) and the National Science Foundation (NSF). It also makes use of data products from the Wide-field Infrared Survey Explorer, which is a joint project of the University of California, Los Angeles, and the Jet Propulsion Laboratory/California Institute of Technology, funded by NASA. UNC-CH gratefully acknowledges NSF awards 0959447, 1009052 and 1211782 for support of Skynet/PROMPT. L.V. and R.L. acknowledge support by CONICYT through the project Anillo ACT-86. A.M. acknowledges the use of C. Harlingten's 20-inch Planewave telescope, which is part of the Searchlight Observatory Network.

Author Contributions F.B.-R. planned the observation campaign, centralized the occultation predictions, participated in the observations, analysed data and results, ran the diffraction and limb-fitting codes, and wrote the paper. B.S. helped to plan the campaign, analysed data and results, wrote and ran the diffraction and limb-fitting codes, and wrote the paper. J.L.O. helped to plan the campaign, analysed data for the occultation prediction, and obtained and analysed data and results. C.S. coordinated and analysed the data from Danish 1.54-m telescope. F. Roques analysed data, and wrote and ran the diffraction and limb-fitting codes. R.V.-M. coordinated the predictions and analysed data. J.I.B.C., F.B.-R., R.V.-M. and M.A. discovered the star candidate and analysed data for the occultation prediction. R.D. coordinated the SOAR and Bosque Alegre observations, and helped to analyse the results. E.J., J.P, R.L., M.E., D.I.M., C.C. and J. Spagnotto obtained and analysed the positive occultation detections from the TRAPPIST, PROMPT, UCO Santa Martina, UEPG, Foz do Iguaçu, Bosque Alegre and Danish telescopes, respectively. E.L. helped to analyse the results. J. Skottfelt, M.G., L. Maquet, N.L., G.B.-R. and A.R.G. helped to obtain the occultation light curves or analysed the data, or both. P.K. ran stellar models to determine the apparent star diameter. H.M. obtained the stellar spectrum. R.S. calculated the short-term ring stability. M.E.M. worked on the confinement mechanisms of the rings. G.T., J.P., A.M., N. Morales, R.G.-H., S.R. and A.C. obtained the negative detections. S.-h.G., X.-b.W., K.H., M.R., J.M., C.O., L.V., L. Mehret, L.L., E.M.S. and R.M. helped to obtain and analyse the positive occultation detections. J.L., F. Colas, F.V., T.W. and K.H. helped to make the predictions and analyse the data. L.A., R.G.S., F. Char, V.P., P.L., N. Martinez, U.G.J., M.D., F. Roig, D.E.R., A.P.L., J.B.H., K.M.I., J.P.M., N.R.F. and D.G.L. were involved in event observations. All authors were given the opportunity to review the results and comment on the manuscript.

Author Information Reprints and permissions information is available at www.nature.com/reprints. The authors declare no competing financial interests. Readers are welcome to comment on the online version of the paper. Correspondence and requests for materials should be addressed to F.B.-R. (ribas@on.br).

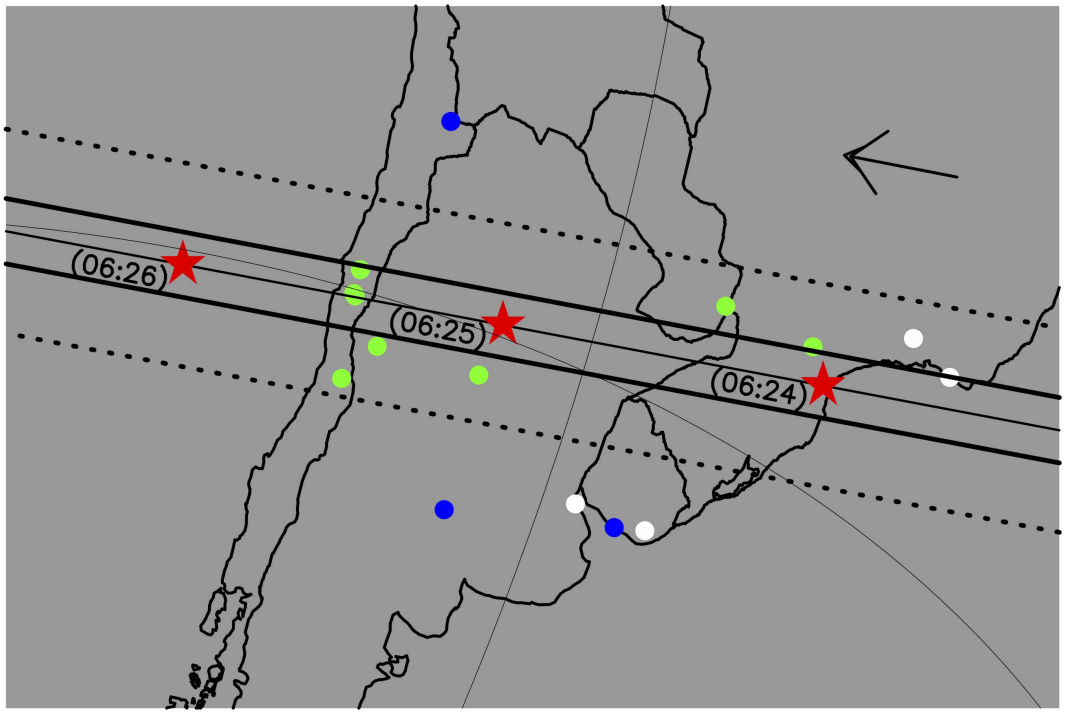

Extended Data Figure 1 | The Chariklo 3 June 2013 occultation campaign. The continuous straight lines indicate Chariklo's shadow track on Earth, and the dotted lines correspond to the ring shadow, as reconstructed from our post-occultation analysis. The shadows move from right to left, as indicated. The red stars indicate the centre of Chariklo's shadow at various times (UTC). The green dots are the sites where the occultation was detected. The blue dots are the sites that had obtained data but did not detect the event, and the white ones are the sites that were clouded out (Extended Data Table 1).

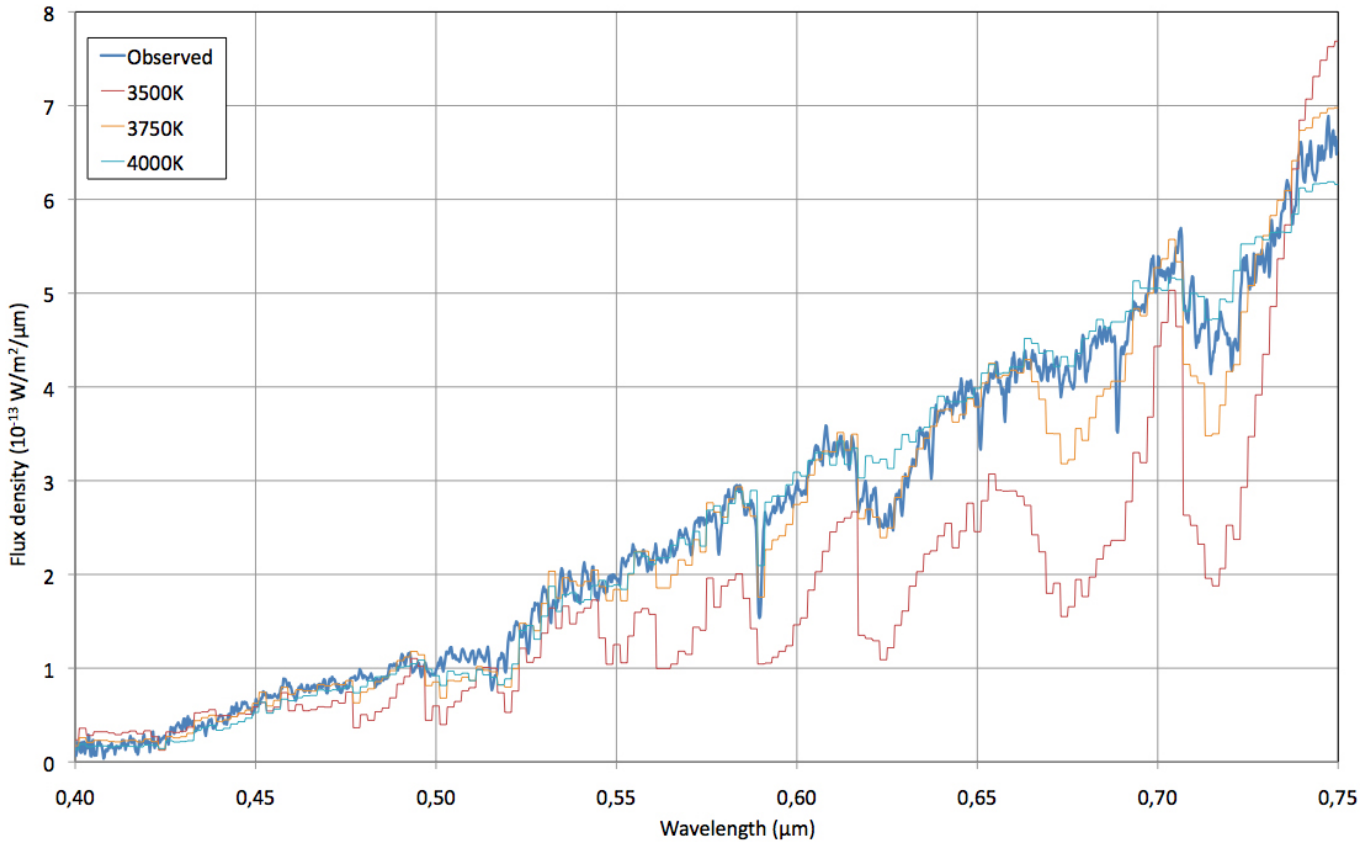

Extended Data Figure 2 | The occulted star spectrum and model. The star spectrum obtained at Pico dos Dias Observatory, Brazil, with the 1.6-m telescope and a Cassegrain spectrograph. Observations were made with the spectrograph configuration, using a grating with 600 lines per millimetre, which gave a resolution of 2.3 Å per pixel covering 3,700–7,700 Å. We obtained three 300-s exposures with a 2-arcsec slit. The calibration was done with the usual procedures and one flux standard star (LTT6248). The thick blue curve represents the observed spectrum. The red, orange and blue thin curves represent ATLAS9 stellar atmosphere models[35] used for comparison (see text).

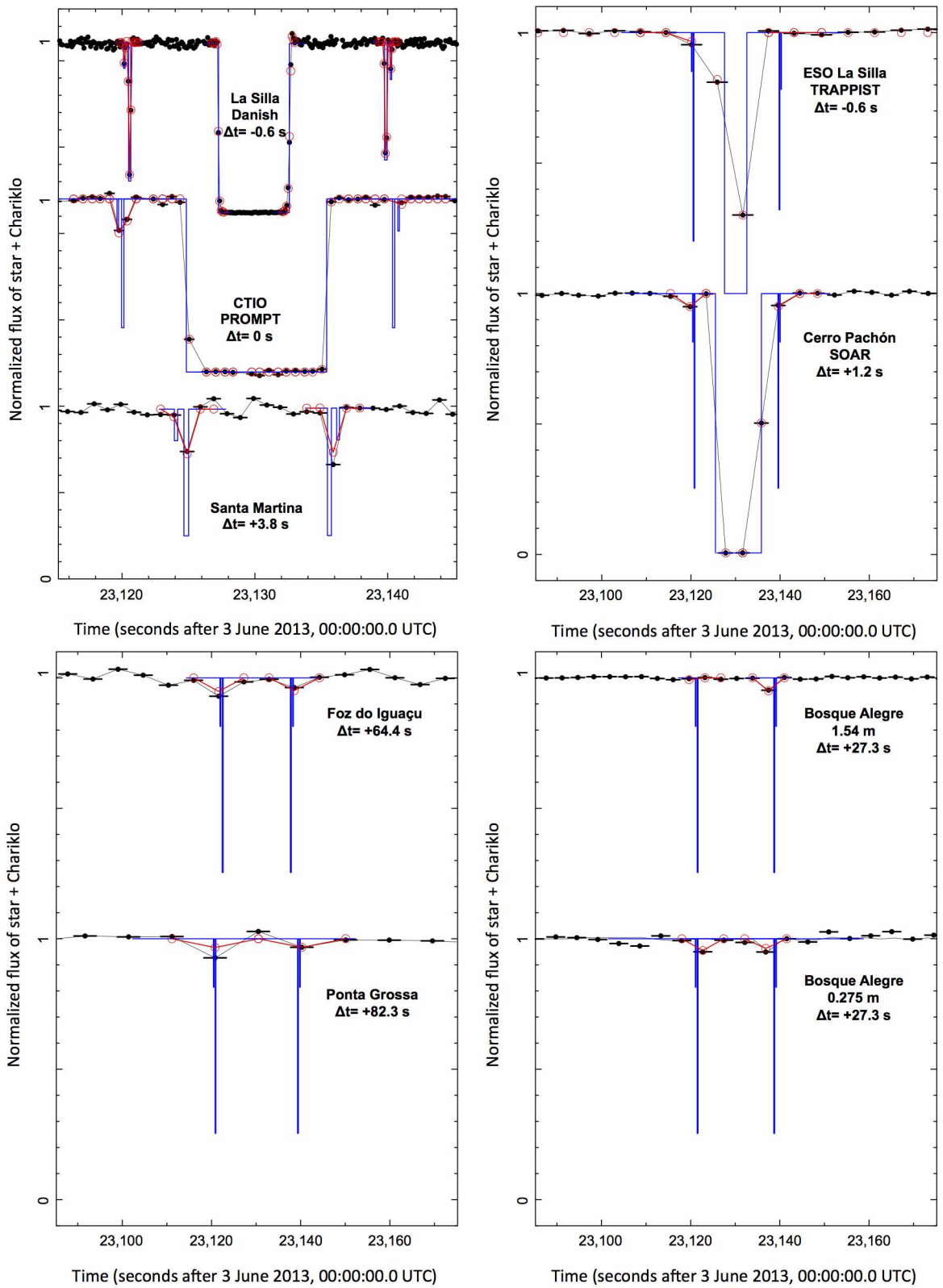

Extended Data Figure 3 | The fits to all the ring and Chariklo events. The black dots are the data points and the horizontal bars indicate the corresponding intervals of acquisition. The light curves are normalized between zero and unity (the latter corresponding to the full flux from the star plus Chariklo), and are shifted vertically for better viewing. They are also displaced in time by the indicated amount Δt, to align the middles of the ring events. The blue curves represent the ring model used to generate the synthetic profiles, which are plotted in red. The ring widths and optical depths for La Silla (Danish and TRAPPIST telescopes) are taken from Extended Data Table 3. For all the other fits, we have used a unique ring model defined by the ring geometry described in Extended Data Table 4, and by the following widths and optical depths: $W_{C1R} = 6.6$ km, $\tau_{N,C1R} = 0.38$, $W_{C2R} = 3.4$ km and $\tau_{N,C2R} = 0.06$ (Extended Data Table 2). An expanded view of the fits to the Danish data is provided in Fig. 3.

Extended Data Table 1 | Circumstances of observations

Site	Coordinates Lat dd:mm:ss Lon dd:mm:ss Altitude (m)	Telescope Name Aperture Filter	Detector Camera Exposure (s) Cycle time (s)	Observers Notes
Main body and ring positive detections.				
La Silla - Chile	29° 15' 21.3" S 70° 44' 20.2" W 2336	Danish 1.54 m Z	Lucky Imager 0.1 0.10091	C. Snodgrass, J. Skottfelt, M. Rabus, U. G. Jorgensen
La Silla - Chile	29° 15' 16.6" S 70° 44' 21.8" W 2315	TRAPPIST 0.6 m no filter	FLI PL3041-BB 4.5 5.7976456 s	E. Jehin C. Opitom Some cycles 6.15-6.19 s
Cerro Tololo* - Chile	30° 10' 03.4" S 70° 48' 19.0" W 2207	PROMPT 0.4 m no filter	U47-MB 0.7 2.0	J. Pollock Some 4 s cycles.
Cerro Pachón - Chile	30° 14' 16.8" S 70° 44' 01.35" W 2738	SOAR 4 m R	SOI 3 3.6–4.6	R. Duffard Unstable cycling.
Ring positive detections.				
Santa Martina† - Chile	33° 16' 09.0" S 70° 32' 04.0" W 1450	M16 0.4 m no filter	Raptor/Merlin127 1.0 1.0016887	R. Leiva Espinoza L. Vanzi
Bosque Alegre - Argentina	31° 35' 54.0" S 64° 32' 58.7" W 1250	EABA 1.54 m no filter	Apogee AU9 3 3.5616717	C. Colazo E.M. Schneiter R. Melia
Bosque Alegre - Argentina	31° 35' 54.0" S 64° 32' 58.7" W 1250	ORBA C11 0.275 m no filter	Apogee AU10 4 4.71	C. Colazo E.M. Schneiter R. Melia
Ponta Grossa - Brazil	25° 05' 22.2" S 50° 05" 56.4' W 909	RCX 400 0.4 m no filter	SBIG STL6E 5 9.78	M. Emilio L. Mehret
Foz do Iguaçu - Brazil	25° 26' 05.4" S 54° 35' 37.4" W 185	C11 0.275 m no filter	SBIG ST-7XME 4 5.65	D. I. Machado L. Lorenzini
Cerro Burek - Argentina	31° 47' 12" S 69° 18' 25" W 2665	ASH 0.45 m no filter	SBIG-STL11000 7 8.4	N. Morales The ring event was marginally detected.
Negative detections.				
Santa Rosa - Argentina	36° 38' 16" S 64° 19' 28" W 182	El Catalejo 0.20 m no filter	Meade DSI-I 5 6	J. Spagnotto
San Pedro de Atacama‡ - Chile	22° 57' 12"S 68° 10' 48" W 2400	Planewave 0.50 m no filter	Apogee U42 2 2.871	A. Muray F. Char B. Sandness
Montevideo - Uruguay	34°45' 20" S 56°11' 23" W 130	OALM 0.46 m no filter	FLI PL0900 2 2.83	S. Roland N. Martinez passing clouds.
The following stations were clouded out during the event.				
Aigua-OAGA / Uruguay; Buenos Aires / Argentina Itajubá-OPD; Rio de Janeiro-ON / Brazil.				

* Three identical telescopes were used (P1, P3, P5), with exposures starting 0.7 s from each other.
† Universidad Catolica Observatory of Santa Martina (UCOSM).
‡ The ASH2 (0.4 m) and ADO (0.38 m) telescopes were also used in this site, with larger cycle times.

Extended Data Table 2 | Timings of the ring events apart from those from the Danish telescope

Site	N†	t^*_{C1R}	χ^2_{dof}	t^*_{C1R}	χ^2_{dof}
		ingress		egress	
Santa Martina	5	23,121.03±0.29	1.48	23,131.811±0.025	4.61
Bosque Alegre/1.54m	3	(23,094.265±0.17)‡	1.08	23,111.44±0.14	0.27
Bosque Alegre/0.275m	3	(23,095.45±1.85)§	0.39	(23,109.45±1.75)§	0.94
SOAR	3	(23,118.8±1.3)‖	1.47	(23,138.4±1.4)‖	0.11
PROMPT	11	23,120.046±0.011	1.06	(23,140.445±0.155)‡	0.81
TRAPPIST	3	23,120.9±1.9	2.99	23,140.88±0.53	2.01
Ponta Grossa	3	23,038.6±2.5	6.70	23,058.0±2.5	1.93
Foz do Iguaçu	3	23,057.5±1.7	1.64	23,074.1±2.0	0.42

Because the Cerro Burek chord does not bring further constraints to our analysis, it is not listed here.
* The fitted time for the middle of C1R, expressed as seconds after 00:00:00 UTC, 3 June 2013, calculated assuming that rings C1R and C2R have widths and optical depths that are averages of the ingress and egress values from the Danish telescopes, that is, $W_{C1R} = 6.6$ km, $\tau_{N,C1R} = 0.38$, $W_{C2R} = 3.4$ km and $\tau_{N,C2R} = 0.06$, and that the radial separation between C1R and C2R is 14.2 km.
† The number of fitted data points.
‡ Obtained from non-detections of the rings (see text).
§ Confirms the ring detection at Bosque Alegre, but is not used in the fit of the ring orbits owing to larger error bars compared with the 1.54-m telescope.
‖ The SOAR timings are probably affected by a systematic offset, and are not used in the fits of the ring orbits and Chariklo's limb shape (see text).

Extended Data Table 3 | Physical parameters of rings C1R and C2R

Ring	N	χ^2_{dof}	t	W (km)	τ_N	E_τ (km)
			ingress			
C1R	10	0.95	23,121.168±0.0007	6.16 ± 0.11	0.449 ± 0.009	2.77 ± 0.04
C2R	8	0.69	23,120.765±0.011	$3.6^{+1.3}_{-2.0}$	$0.05^{+0.06}_{-0.01}$	0.18 ± 0.03
Radial separation (C2R minus C1R): 14.6±0.4 km						
Gap between rings C1R and C2R:				9.0±0.4 km	$\tau_N < 0.004$	E_τ <0.04 km
			egress			
C1R	10	1.19	23,140.462±0.0012	7.17 ± 0.14	0.317 ± 0.008	2.28 ± 0.03
C2R	8	0.71	23,140.847±0.006	$3.4^{+1.1}_{-1.4}$	$0.07^{+0.05}_{-0.03}$	0.24 ± 0.02
Radial separation (C2R minus C1R): 14.1±0.2 km						
Gap between rings C1R and C2R:				8.3±0.2 km	$\tau_N < 0.004$	E_τ <0.05 km

N, number of fitted data points (there are $M = 3$ free parameters: t, W and τ_N); $\chi^2_{\mathrm{dof}} = \chi^2/(N-M)$, the χ^2 per degree of freedom; t, mid times of ring events, in seconds after 00:00:00 UTC, 3 June 2013. W, radial width, measured in the plane of the rings (using the ring pole given in Table 1); τ_N, normal optical depth; $E_\tau = W\tau_N$, equivalent depth. The error bars quoted here are internal to the fits, and are given at the 1σ level. The error bars in absolute time, ±0.014 s, are larger than the error bars on the relative times reported here (see text).

Extended Data Table 4 | Ring geometry

Elliptical fit to the ring events, projected in the plane of the sky Number of ring positions fitted: 14, number of adjusted parameters: 5, $\chi^2_{\rm dof} = 1.48$					
f_c (km)	g_c (km)	a (km)	e	B (deg)	P (deg)
-2734.7±0.5	+793.8±1.4	390.6±3.3	0.444±0.006	+33.77±0.41	**-61.54±0.14** or 118.46±0.14
	Ring pole (equatorial J2000)				
	Right ascension, α_p	Declination, δ_p			
	10 h 05.2 min ± 2.0 min	**41° 29' ± 13'**	**Solution 1 (preferred, see text)**		
	01 h 47.8 min ± 1.2 min	03° 26' ± 19'	Solution 2		

The elliptical fit uses the timings and associated error bars of Extended Data Table 2, and the methodology used in previous works[18,20]. Definitions of listed parameters are as follows (see text). By (f_c, g_c) we denote the centre of the ring in the plane of the sky, with the two coordinates counted positively towards local celestial east and north, respectively. This is the offset to apply to Chariklo's ephemeris to fit the observations. Transformation to arc seconds can be performed using a geocentric distance $D = 2.031 \times 10^9$ km during the occultation. Here we use the star position given in equation (1) of the Supplementary Information and the JPL#20 Chariklo ephemeris. By a we denote the apparent semi-major axis of the ring projected in the plane of the sky; by e, the aspect ratio of the ring, $e = (a - b)/a$, where b is the apparent semi-minor axis of the ring projected in the plane of the sky; and by P, the position angle defining the angle between celestial north and the semi-minor axis of the ring projected in the plane of the sky, counted positively from celestial north to celestial east. By convention, it refers to the projected semi-major axis that corresponds to superior conjunction. By B we denote the ring opening angle, calculated from $|\sin(B)| = 1 - e$. Equivalently, it is the absolute value of the elevation of the observer above the ring plane.

Extended Data Table 5 | Timings of the Chariklo event

Site	N	ingress	χ^2_{dof}	egress	N	χ^2_{dof}
Danish*	10	23,127.861±0.014	0.30	23,133.188±0.014	10	3.3
TRAPPIST	9	23,127.893±0.019	0.84	23,133.155±0.007	10	1.47
PROMPT	22	23,124.835±0.009	0.71	23,135.402±0.015	26	0.58
SOAR†	3	(23,124.34±0.59)	0.72	(23,134.597±0.009)	3	0.57

* These timings were corrected by −1.622 s using the TRAPPIST times (see text).
† These timings may be affected by a delay of about 0.5 s, and are not used for Chariklo's limb fitting (see text).

Extended Data Table 6 | Chariklo physical properties

f_c (km)*	g_c (km)*	R_{eq} (km)	R_{equiv} (km)†	e	P (deg)*
-2734.7±0.5	+793.8±1.4	144.9±0.2	126.9±0.2	0.213±0.002	-61.54±0.14

Geocentric position derived from the occultation (J2000)‡		
Time (UT)	Right Ascension	Declination
06:30:00	$16^h\ 56^{min}\ 06.4618^s \pm 0.006^s$	$-40°31'\ 30.009'' \pm 0.002''$

* The centre and position angle of the elliptical fit to the Chariklo chords were taken from the ring fit (Extended Data Table 4).
† $R_{equiv} = R_{eq}\sqrt{1-e}$ is the radius of a circle having the same apparent area as the fitted ellipse.
‡ The error is largely dominated by the star-position error determination, not by the limb fit.